Pergamon

Int. J. Solids Structures Vol. 34, Nos. 35–36, pp. 4617–4631, 1997

0020–7683/97 $17.00 + .00

PII: S0020–7683(97)00043–7

AXISYMMETRIC DELAMINATION IN DEPOSITED MULTI-LAYERS

S. H. NARAYAN and J. L. BEUTH
Department of Mechanical Engineering, Carnegie Mellon University, Pittsburgh, Pennsylvania 15213, U.S.A.

(*Received* 8 *August* 1995; *in revised form* 25 *May* 1996)

Abstract—The problem of residual stress-driven axisymmetric delamination in successively deposited isotropic multi-layers is addressed in this study. A circular-shaped multi-layer is modeled with a delamination crack extending uniformly from the free edge. Applications for this work include the modeling of residual stress-driven delamination of multi-layered coatings and films. The application of specific interest is residual stress-driven debonding in parts created by layered manufacturing methods, where molten metal layers are successively deposited to form three-dimensional shapes. Results for energy release rates as a function of delamination crack length are presented from fracture mechanics models of various axisymmetric multi-layer geometries. Results are compared to those from planar delamination problems. Methods are outlined for determining a conservative upper bound for the maximum energy release rate for an axisymmetrically extending delamination crack. These methods are based on potential energy calculations from a residual stress model for an uncracked multi-layer and do not require fracture mechanics modeling. The easily calculated bound for the maximum energy release rate can be used to guide the design of delamination-resistant multi-layers. © 1997 Elsevier Science Ltd.

1. INTRODUCTION

This study addresses the problem of residual stress-driven axisymmetric delamination of successively deposited isotropic multi-layers. The term successively deposited is used to designate that each layer has experienced free thermal contractions relative to the layers below it. Applications of the methods outlined in this work include the analysis of delamination problems in electronic components such as integrated circuits, hard disk drives and electronic packaging. The manufacture of these components typically involves the deposition of multiple layers or films at elevated temperatures. Similarly, methods from this study can be applied to the delamination or peeling of multi-layered coatings, such as those used to protect metal parts from corrosion. In many applications of these types and in multi-layered test specimens, an understanding is needed of delamination of axisymmetric geometries.

The application serving as the principal motivation for this work is the problem of delamination in parts built using rapid prototyping-based layered manufacturing processes (see Marcus and Bourell (1993)). These processes involve the construction of three-dimensional parts by first creating a computed-aided design (CAD) drawing of the part to be built. The drawing is electronically sectioned into layers and the 3-D part is then built by successive layer deposition. The goal of these processes is to transition from the creation of a 3-D polymer model of a part (an established technology of which stereolithography is an example) to the creation of actual parts made of one or more metals.

The particular process of interest for this work has been termed shape deposition manufacturing (see Prinz *et al.* (1995)). This process involves layer deposition followed by computer numerically controlled machining of that layer to shape. The deposition method currently used in this process has been termed microcasting. In microcasting, material is deposited onto existing layers of a part in the form of molten metal droplets. The radius of each molten droplet is comparable to the layer thickness, which is on the order of 2 mm. The microcasting process gives rise to residual stresses, which can lead to delamination at layer interfaces. As noted in Chin *et al.* (1995), residual stress build up during this process is complicated. It includes effects of both the contraction of individual droplets and the

thermal loading of existing material by deposited droplets. The stress model used to demonstrate the methods of this study will not accurately represent the stress distributions in actual microcast parts; however, once accurate stress models are fully developed for this process, they can be used with the methods outlined in this study.

Although three-dimensional parts created using layered manufacturing methods can be of arbitrary shape, it is typical for parts to include some features that can be modeled as two-dimensional. These include thin-wall and rectangular plate features as well as circular plate features with axisymmetric symmetry. This study addresses axisymmetric delamination geometries. Delamination of thin-walled and rectangular plate geometries has been addressed in Beuth and Narayan (1996). In addition to direct application of the results of this study to axisymmetric features in three-dimensional parts, the methods developed here also have relevance to fully three-dimensional delamination problems. It is shown in this study that the energy release rate behavior of axisymmetric delamination problems is more complicated than that observed in planar geometries. An understanding of the axisymmetric problem is gained, however, by considering appropriate steady-state energy release rates. Although it is not pursued in this study, it is likely that insights could also be gained in fully three-dimensional delamination problems by similar comparisons of observed energy release rates with steady-state energy release rates.

The axisymmetric configuration considered in the present work is related to two planar two-dimensional multi-layer debonding geometries studied by Beuth and Narayan (1996). These two planar problems and the axisymmetric problem are illustrated in Fig. 1, which shows three four-layer configurations with debonding taking place at the mid-plane of each multi-layer. In the problem illustrated in Fig. 1a, delamination occurs in a thin-walled multi-layer, with a crack of uniform length, a, extending from the free edge. Because the multi-layer is thin, each layer is in a state of plane stress, with a uniaxial state of stress (σ_{xx}) in each layer away from the crack front and the free edges. In Beuth and Narayan (1996) it is demonstrated that for a sufficiently long delamination crack, the crack tip energy release rate, G, reaches a constant (steady-state) value, designated as G_{ss}. Furthermore, G_{ss} can be calculated using only a model of residual stress for uncracked multi-layers. Thus, a fracture mechanics model of the problem (e.g., a finite element model of the cracked multi-layer) is not needed.

The second type of two-dimensional delamination problem is similar to the first; however, the geometry is that of a multi-layered rectangular plate (Fig. 1b) instead of a thin wall. A delamination crack has initiated at the free edge and is propagating with a crack front that is parallel to the z axis. For this type of problem (see Beuth and Narayan (1996)), free thermal contractions which are independent of location in the plane of the deposited layers result in a biaxial state of residual stress ($\sigma_{xx} = \sigma_{zz}$) in each layer, away from the crack front and the free edges. As in the thin-wall configuration, the crack tip energy release rate reaches a steady-state value for a sufficiently long crack and this value, designated in this study as G_{ss}^{plate}, can be calculated without use of a fracture mechanics model.

The third problem type, which is analyzed in the present work, is an axisymmetric configuration consisting of a circular multi-layer with the crack front initiating at the free edge and moving toward the multi-layer center (Fig. 1c). As in the rectangular plate problem of Fig. 1b, free thermal contractions result in a biaxial state of stress ($\sigma_{rr} = \sigma_{\theta\theta}$) in each layer, away from the crack front and the free edges. It is shown, however, that unlike the problems of Figs 1a and 1b, the energy release rate of the delamination crack does not reach a constant value for long crack lengths.

This study not only builds on previous work on multi-layers by the authors, but also on work by others in modeling the debonding of single thin films. As in multi-layer problems, debonding of thin, bonded single films can be divided into planar (thin-wall or rectangular plate) and axisymmetric configurations. The idea of seeking easy-to-calculate constant (steady-state) energy release rates for such problems is articulated in the review paper by Hutchinson and Suo (1991). Steady-state concepts are directly applicable to planar problems of thin, bonded films in tension. Examples of the application of steady-state concepts to tensile film debonding include the work of Drory *et al.* (1988) and Evans

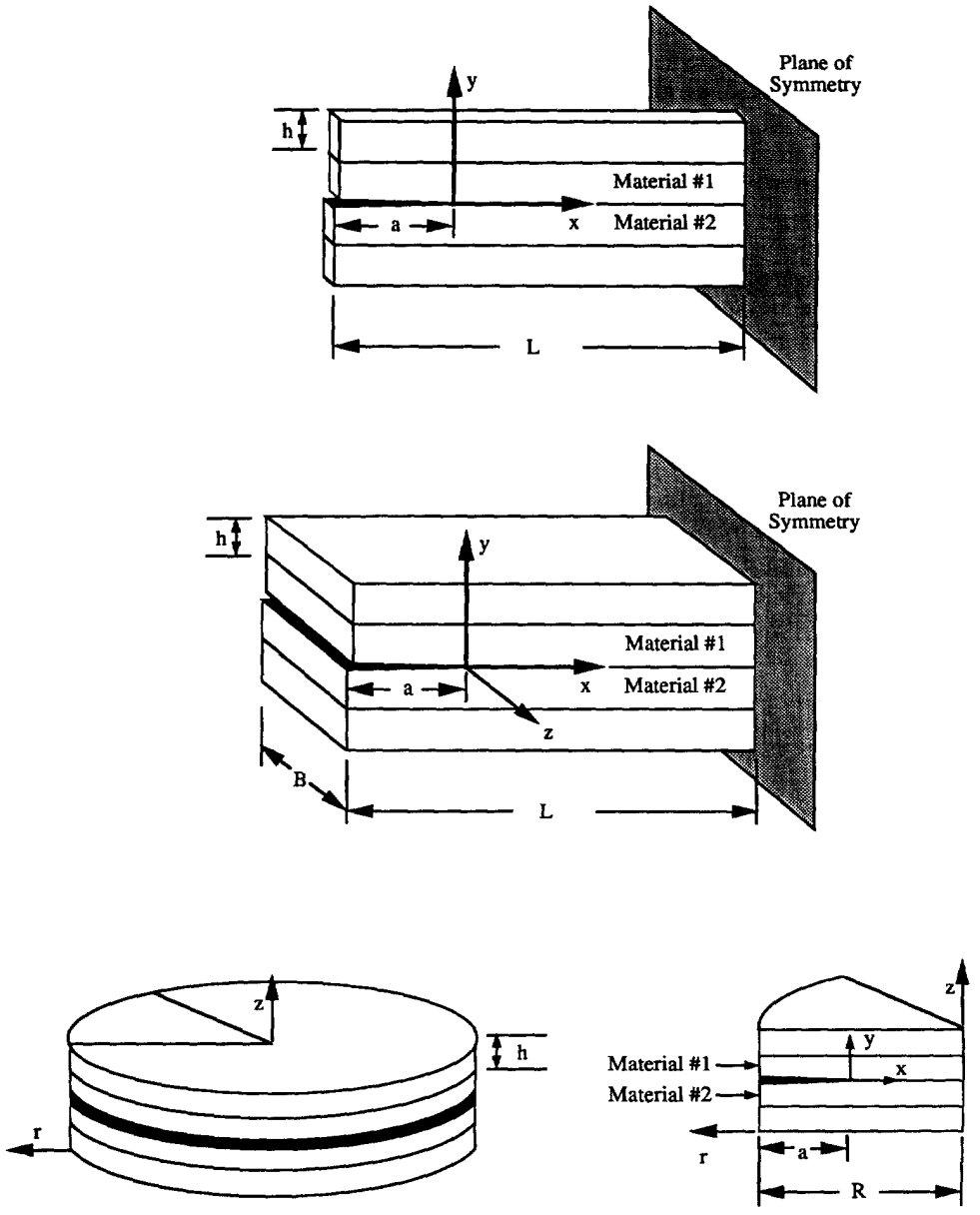

Fig. 1. (a) Planar delamination: plane stress (b) planar delamination: biaxial stress and (c) axisymmetric delamination: biaxial stress.

et al. (1988). In the thin film problem (as opposed to the multi-layer problem) formulae for steady-state energy release rates take simple forms due to assumptions of uniform stress in the film, no stress in the substrate material and the fact that debonded portions of the film as stress free. The concept of steady-state cracking is generally not applicable to problems of planar debonding of thin films in compression (see, for example, Evans and Hutchinson (1984), Jensen (1993) and Stringfellow and Freund (1993)). In compression, debonding occurs by film buckling away from the free edges. Such failures do not result in steady-state energy release rates for long cracks.

Delaminations having axisymmetric geometries can occur in thin, bonded films in the presence of biaxial stress. In compression, the failure geometry is one of blister-shaped spalling and, as in compressive planar geometries, steady-state behavior is not observed (see Hutchinson, Thouless and Liniger (1992)). In thin, bonded films in tension, the geometry is analogous to the multi-layer geometry shown in Fig. 1c, with a circular crack front moving from the edge of the film toward its center. The energy release rate behavior

of such problems is demonstrated by Drory *et al.* (1988) and Evans *et al.* (1988). In contrast to the planar problem, the axisymmetric film debonding problem exhibits energy release rates that increase steadily with crack length, until the film has almost completely debonded from the substrate. Explanations for the observed differences in energy release rate behavior for planar and axisymmetric problems have not been offered in the literature, even for the simple case of thin film debonding. Similarly, no attempts have been made to quantify axisymmetric energy release rates in ways analogous to those for steady-state energy release rates of planar problems.

The current study addresses the need in the literature for an understanding of axisymmetric delamination in multi-layers. This work not only demonstrates the nature of the energy release rate behavior for such problems, but also offers explanations of observed behavior and methods for approximating it based on its relation to that of the planar, steady-state problem. A detailed problem description is given in the next section. A description is then given of the finite element model used to determine energy release rates for axisymmetrically extending delamination cracks. Energy release rate results are presented as a function of delamination crack length for various multi-layer configurations. The numerical results are followed by an analysis of the problem, leading to the determination of a conservative upper bound for the maximum energy release rate for an axisymmetrically extending delamination crack, designated as $G_{\max}^{\text{limit}}$. Values for $G_{\max}^{\text{limit}}$ can be calculated without performing a fracture analysis of the problem and can substantially simplify the task of designing delamination-resistant axisymmetric multi-layer stacking geometries.

2. PROBLEM DESCRIPTION

The geometry of the axisymmetric delamination problem is illustrated in Fig. 1c, which shows a circular multi-layer with a residual stress-driven delamination crack of length a (see the cut-out portion of the figure) extending uniformly from the free edge. Both global (r and z) and crack tip (x and y) coordinates are designated in the figure. Each layer may be of a different material. Although the delamination is illustrated in Fig. 1c as occurring on the mid-plane interface, it may occur along any interface in the multi-layer. Residual stresses in the multi-layer are assumed to be the result of deposition of each layer onto the (existing) layers below it. The key assumption made in this study is that free thermal contractions resulting from layer deposition are independent of the r and θ coordinates. This results in an r- and θ-independent biaxial stress state within the multi-layer, away from the delamination front and the free edges.

The techniques outlined in this study can be applied to any multi-layer delamination problem of the type just described. However, in this study a specific sub-class of problems is modeled, which serves to illustrate the generic attributes of all problems of this type. In all of the cases presented in this work, successive deposition is modeled by assuming that each layer experiences a uniform (independent of not only r and θ but also z) free thermal contraction (characterized by a free thermal strain $\alpha\Delta T$) relative to the layers below it. It is assumed that residual stress build up in the multi-layer is elastic. It is also assumed that all layers are deposited and cooled to room temperature before any bending deformation takes place. This final assumption models a multi-layer which is fully constrained from bending deformation during its construction, but is then released upon completion. This constraint condition is close to actual constraint conditions applied in shape deposition manufacturing, the application motivating the present work.

3. NUMERICAL METHOD

The finite element model used in this study is illustrated in Fig. 2, which shows a typical deformed element mesh. The model consists of eight-noded axisymmetric biquadratic displacement interpolation elements generated using the finite element package ABAQUS. The model illustrated consists of four layers of equal thickness, h, with the crack located at the mid-plane of the multi-layer. The right edge defines the z axis of the model, where boundary conditions of zero radial displacement are applied. A refined mesh is used near

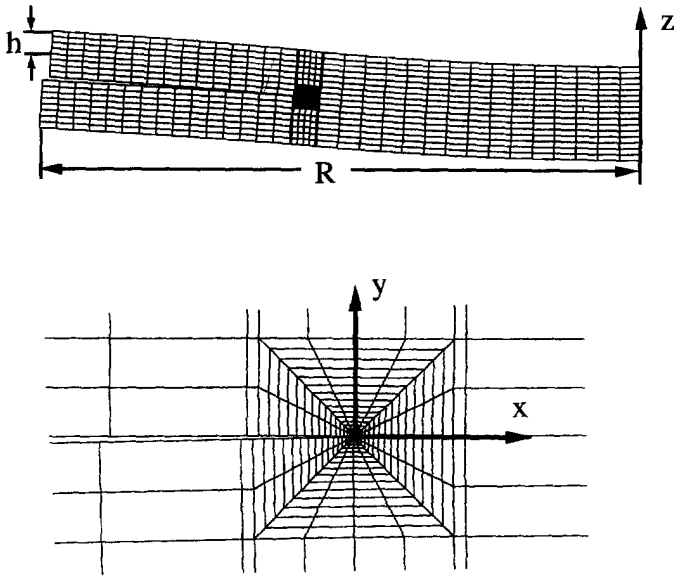

Fig. 2. Far-field and near-tip finite element meshes for a four-layer axisymmetric problem.

the crack tip, which has elements focused toward the tip. Quarter-point elements are used at the crack tip to capture the $1/\sqrt{r}$ near-tip strain dependence. For the results presented in this study, the near tip mesh consists of 18 rings of elements meshed over a length equal to half the layer thickness. Energy release rate results for various material combinations and multi-layer geometries are presented in the next section. Energy release rates are extracted from the model using multiple J contour integrals evaluated near the crack tip. Essentially path-independent J integral values are observed outside of the first or second ring of elements around the crack tip and these are the values reported in this study.

4. NUMERICAL RESULTS

In this section, results for energy release rates as a function of crack length are presented for various axisymmetric multi-layer delamination problems. In order to limit the number of cases studied, only two-layer and four-layer configurations with layers of equal thickness, h, are modeled. In order to demonstrate the relationship between planar and axisymmetric problems, axisymmetric energy release rate results are compared to those for plane stress (thin-wall) planar delamination problems (Fig. 1a) having the same layering configuration.

The energy release rate behavior of multi-layer delamination problems having planar geometries (Figs 1a and 1b) is detailed in Beuth and Narayan (1996). Because it is related to the axisymmetric problem, a brief overview of planar delamination is given here. In the planar problems illustrated in Figs 1a and 1b, it is assumed that material in each layer has experienced a free thermal contraction with respect to the layers below it and that this contraction is independent of the x coordinate. Under such conditions, for a sufficiently long delamination crack, the near-crack-tip stress distribution simply translates in the x direction as the crack extends. This steady-state condition results in a constant-valued energy release rate, designated in this study as G_{ss} or G_{ss}^{plate} for the problems of Fig. 1a or 1b, respectively. By definition, the energy release rate, G, is the potential energy released per unit newly created crack surface. The steady-state energy release rate can thus be calculated as the difference in potential energy per unit width per unit length between portions of the multi-layer far ahead of and far behind the crack tip. A solution that models the near-crack-tip fields is not needed for this calculation; instead, a model of the residual stress state in each layer of an uncracked multi-layer can be used. The residual stress model also does not need to model stresses near the free edges of the layer.

All of the cases analyzed in this study assume a uniform free thermal contraction within each layer and elastic material response. Under such assumptions, residual stresses

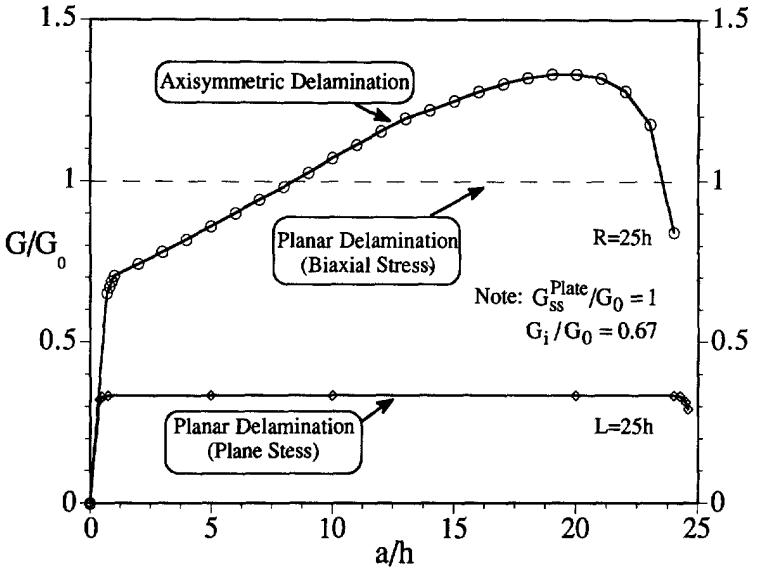

Fig. 3. Normalized G vs normalized crack length for two-layer axisymmetric and planar delamination problems, with $E_1/E_2 = 1$ and $\nu_1 = \nu_2 = 0.33$.

in an uncracked multi-layer can be approximated by a multi-layer generalization of the solution by Timoshenko (1925) for the stresses in a uniformly heated bimaterial strip. This model assumes that each layer experiences a uniform free thermal strain (characterized by $\alpha\Delta T$) relative to the layer below it. As in the Timoshenko model, layers behave as beams or plates with linear stress variations through the thickness of each layer. It is shown in Beuth and Narayan (1996) that a Timoshenko-based model can be applied to predict G_{ss} and G_{ss}^{plate} for the problems of Figs 1a and 1b. Furthermore, G_{ss} and G_{ss}^{plate} are related by the formula

$$G_{ss}^{plate} = \frac{2G_{ss}}{1-\nu}. \tag{1}$$

The factor $2/(1\text{-}\nu)$ arises from the biaxial far-field stress state in the rectangular plate problem, where two stresses of equal magnitude (σ_{xx} and σ_{zz}) are released by the extension of the delamination crack.

The energy release rate behavior for a thin-wall planar delamination problem (Fig. 1a) is illustrated by results plotted in Fig. 3 for debonding of two layers, each of thickness h, having the same elastic properties E and ν. The model used is symmetric, modeling delaminations extending inward simultaneously from two edges. The half-length, L, of the model is $25h$. The figure gives normalized energy released rate (the normalization is described below) obtained from a finite element fracture model of this configuration, plotted as a function of normalized crack length a/h. The figure shows that for this planar problem, the steady-state energy release rate is reached within $a/h = 1$ and is maintained until the part is almost separated into two pieces. Also, the steady-state energy release rate (G_{ss}) value obtained from the finite element fracture model is accurately predicted using a Timoshenko-based model to calculate the potential energy differences between bonded and debonded parts.

Identical arguments can be applied to rectangular plate planar delamination problems (Fig. 1b), except that values of G_{ss}^{plate} are scaled by the factor $2/(1-\nu)$ as indicated by eqn (1). In Fig. 3 (and in plots for other cases presented in this paper) the value of G_{ss}^{plate} calculated using a Timoshenko-based model is designated by a dashed line. Calculation of G_{ss} and G_{ss}^{plate} values is straightforward for any multi-layered configuration and details for calculating G_{ss}^{plate} for the problem of Fig. 3 are presented here as an example. For the two-layer case in Fig. 3, because the debonded portions of the multi-layer away from the crack

front are stress free, G_{ss}^{plate} is just the strain energy per unit length per unit width in the two-layered part. A Timoshenko (1925) bimaterial strip analysis of this configuration gives the following stress distribution in the fully bonded two-layer part, valid away from the free edges:

$$\sigma = \sigma_{xx} = \sigma_{zz} = \frac{E}{(1-\nu)}\alpha\Delta T(-1/2-3/4\, y/h) \quad \text{(bottom layer)},$$

$$\sigma = \sigma_{xx} = \sigma_{zz} = \frac{E}{(1-\nu)}\alpha\Delta T(1/2-3/4\, y/h) \quad \text{(top layer)}. \tag{2}$$

In eqn (2), $y = 0$ corresponds to the layer interface (y varies from $-h$ to 0 for the bottom layer and from 0 to $+h$ for the top layer). The strain energy in the two-layer part is given by

$$SE = \left(\frac{1-\nu}{E}\right)\int \sigma^2 \, \mathrm{d}V. \tag{3}$$

Substituting for σ and integrating over one half of the symmetric part gives

$$SE = \frac{E}{16(1-\nu)}(\alpha\Delta T)^2 HBL, \tag{4}$$

where B is the part width, L is the half-model length and $H = 2h$ is the total thickness of the part. This yields a value for G_{ss}^{plate} of:

$$G_{\text{ss}}^{\text{plate}} = \frac{E}{16(1-\nu)}(\alpha\Delta\text{T})^2 H. \tag{5}$$

Calculation of G_{ss}^{plate} for other configurations is similar. For multiple layers, the difference between the potential energies of a fully bonded multi-layer and the debonded portions is needed to determine G_{ss}^{plate}.

In the results presented in this paper, energy release rates are normalized with respect to the G_{ss}^{plate} value of eqn (5), with definitions generalized for application to multi-layer configurations. The energy release rate normalization parameter is

$$G_0 = \frac{\overline{E_{\text{avg}}}}{16}(\alpha\Delta T)^2 H, \tag{6}$$

where H is the total thickness of the part under consideration and $\alpha\Delta T$ is the free thermal strain mismatch between the layers (which is taken to be the same between all layers in the four-layer cases studied in this paper). $\overline{E_{avg}}$ is defined as $\overline{E_{avg}} = \Sigma(E_i h_i)/(H(1-\nu_i))$. The Poisson's ratio, ν is taken to be 0.33 for all layers in the cases presented in this study.

In Fig. 3, normalized energy release rates are also plotted for the same two-layer configuration, but with an axisymmetrically extending crack as illustrated in Fig. 1c. Here the radius of the circular multi-layer, R, equals $25h$. The plot shows that for the axisymmetric problem, outside of the short crack regime, G increases steadily with a/h until the remaining crack ligament becomes small. G then reduces to zero as the crack length is increased further. The maximum energy release rate for the axisymmetric problem, designated in this study as $G_{\max}$, is higher than the steady-state energy release rate, G_{ss}^{plate}. The transition from short crack behavior occurs within $a/h \leqslant 1$, as in the plane stress planar problem. However, the decay of G from its maximum value occurs over a larger crack length compared to the plane stress planar problem.

The behavior for the axisymmetric problem of Fig. 3 is typical and is caused by the non-uniform manner in which the radial and circumferential stresses, σ_{rr} and $\sigma_{\theta\theta}$, are

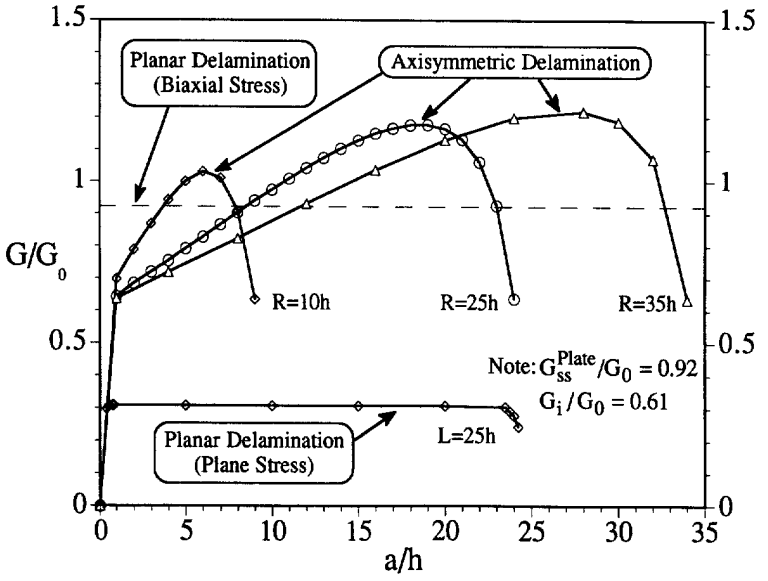

Fig. 4. Normalized G vs normalized crack length for two-layer axisymmetric and planar delamination problems, with $E_1/E_2 = 1/3$ and $\nu_1 = \nu_2 = 0.33$.

released by the extending axisymmetric crack. For short crack lengths, radial stress (σ_{rr}) is released by the extending crack, but due to circumferential constraint behind the crack front, circumferential stress ($\sigma_{\theta\theta}$) is not. The energy release rate corresponding to the release of a single stress in the presence of a biaxial stress state $\sigma_{rr} = \sigma_{\theta\theta}$ is designated as G_i in the note of Fig. 3 and in the other energy release rate plots presented in this study. This "initial" energy release rate, G_i, is also used in the Analysis section of this paper to help determine an upper bound for the maximum energy release rate for an axisymmetrically extending delamination. As the crack length is increased, the contribution of $\sigma_{\theta\theta}$ to the energy release rate increases due to gradual relaxation of the circumferential constraint behind the crack front. This causes the observed steady increase in energy release rates with increasing a/h.

Figure 4 gives a plot of normalized G vs a/h for delamination of two axisymmetric layers with the stiffness, $\bar{E} = E/(1-\nu)$, of the lower layer three times that of the upper layer. Three circular multi-layers with radii of $10h$, $25h$ and $35h$ are considered for comparison. In all three cases, behavior similar to that shown in Fig. 3 is observed, with energy release rates increasing steadily with a/h, then reaching a maximum before falling to zero as a/h approaches R. Because strain energies do not scale proportionally with $\bar{E}_{avg}$, normalized energy release rates are lower than those of Fig. 3. For the case $R = 25h$, the crack length over which a transition is made to steadily increasing energy release rates for short cracks is greater in Fig. 4 than in Fig. 3. Similarly, the crack length over which the energy release rate falls from its peak value to zero for long cracks is greater in Fig. 4 than in Fig. 3. The maximum energy release rate for the $R = 25h$ case shown in Fig. 4 occurs at $a/h = 19$, compared to $a/h = 20$ for the previous problems with no elastic mismatch (Fig. 3). This parallels behavior observed in planar delamination problems (including the planar results plotted in Figs 3 and 4), where the transition to and from steady-state conditions occurs over greater crack lengths as material mismatches are increased. As mismatches are increased, the effects of free edges exist at greater distances into a part. Similarly, for cases of large material mismatch a larger uncracked ligament length or radius is needed to achieve full thermal mismatch stresses ahead of the crack tip.

In all of the plots of Fig. 4 (including that for the planar problem), the transition from short crack behavior takes place within $a/h \leqslant 1$. Also, for short crack lengths, energy release rates for all three cases in Fig. 4 approach a single value as the crack length is decreased (before falling to zero) and this value corresponds to G_i. This occurs because in the short crack regime, each of the problems is essentially the same, with a single stress being released due to crack extension. In comparing the axisymmetric cases plotted in Fig. 4, however, it

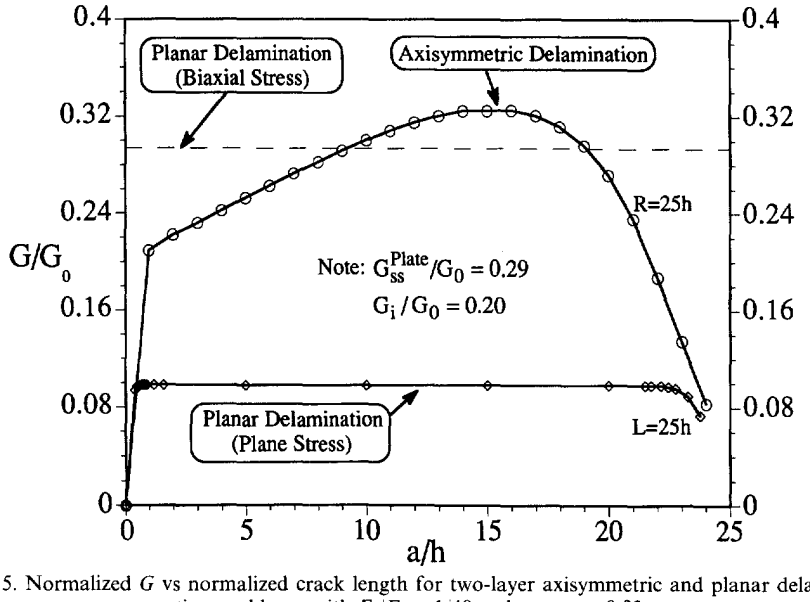

Fig. 5. Normalized G vs normalized crack length for two-layer axisymmetric and planar delamination problems, with $E_1/E_2 = 1/40$ and $\nu_1 = \nu_2 = 0.33$.

is clear that the crack lengths over which energy release rates decay from their maximum values and the G_{max} values themselves are a function of part radius. The decrease in energy release rate from a value of G_{max} when the uncracked ligament becomes small is due to a complex interaction between increasing release of $\sigma_{\theta\theta}$ behind the crack front, which increases G, and the decline in G caused by reduction of uncracked ligament radius. Predicting the crack length at which $G = G_{max}$ would be difficult. In the plots of Fig. 4, it is apparent, however, that the crack lengths over which G falls from G_{max} to zero increase with increasing R and that the dependence of this long crack behavior on multi-layer radius is most pronounced for small values of R (i.e., $R \leqslant 10$h). Values of G_{max} also increase with increasing R/h. This can be explained by the fact that as the multi-layer radius is increased, the regions in the multi-layer near the free edge become a smaller fraction of the part volume. This causes the average energy release rate due to complete debonding of the multi-layer (defined as the total potential energy released in completely separating the multi-layer divided by total debonded area) to increase with increasing part radius, which in turn causes G_{max} to increase. In the Analysis section of this paper, it is shown that the limiting value of average energy release rate for large radius multi-layers is simply G_{ss}^{plate}. An upper bound for G_{max} is derived in terms of G_i and G_{ss}^{plate} and this upper bound is approached as the part radius is increased.

Figure 5 provides a plot of normalized G vs a/h for the case of two axisymmetric layers with an extreme case of elastic mismatch. The stiffness, $\bar{E}$, of the bottom layer is 40 times that of the top layer. Trends with respect to stiffness mismatch observed between Figs 3 and 4 are continued in Fig. 5. The low values of the normalized energy release rates are again due to the fact that strain energies in two-layer problems do not scale proportionally with $\overline{E_{avg}}$. The decline of G from G_{max} for this case is over a larger a/h with G_{max} occurring at $a/h = 16$.

Figures 6 and 7 provide plots of normalized energy release rates for two representative four-layer configurations. Both multi-layers consist of alternating material layers, with each layer having the same thickness. In both cases, it is assumed that the free strain mismatch, characterized by an $\alpha\Delta T$, is the same between each layer. This was done in the numerical model by specifying that each layer have the same coefficient of thermal expansion, α, and using the same temperature mismatch, ΔT, between individual layers. In modeling successive deposition of layers in actual multi-layer configurations, appropriate values of $\alpha\Delta T$ would be specified based on superposition arguments used to model the successive deposition of each layer, coupled with known layer coefficients of thermal expansion and layer temperature changes.

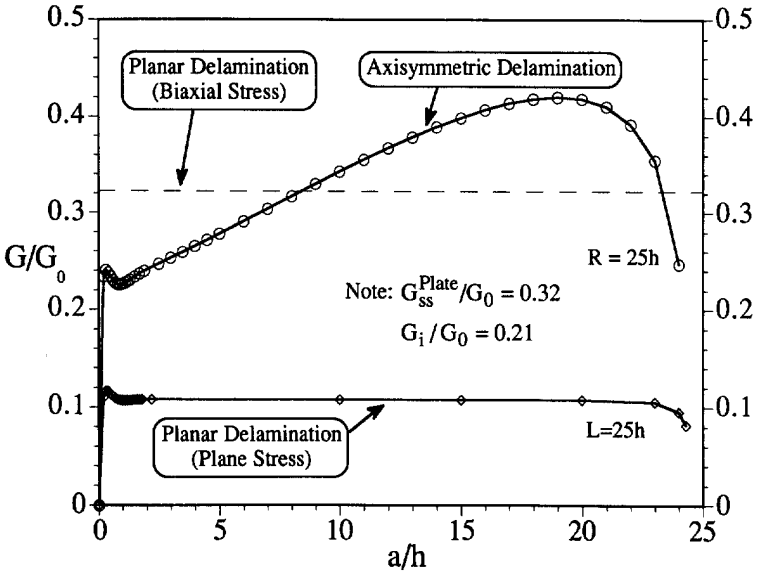

Fig. 6. Normalized G vs normalized crack length for four-layer axisymmetric and planar mid-plane delamination problems, with $E_1/E_2 = 1/3$ and $\nu_1 = \nu_2 = 0.33$.

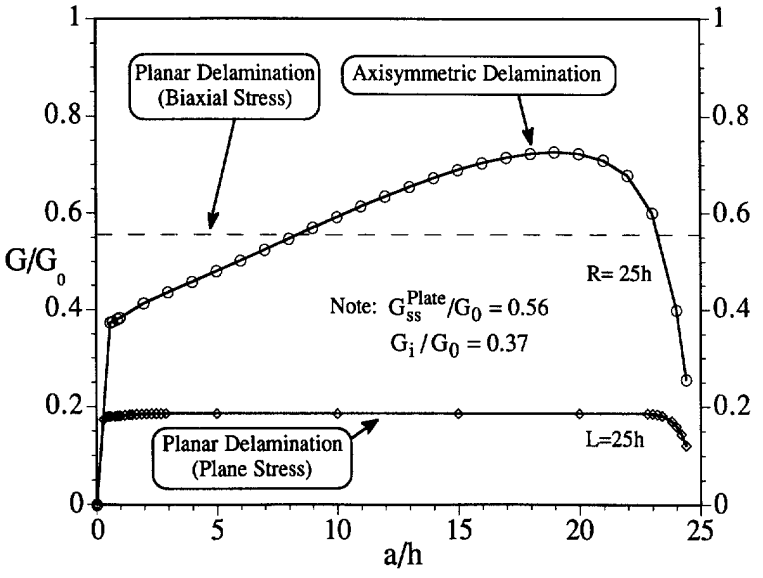

Fig. 7. Normalized G vs normalized crack length for four-layer axisymmetric and planar problems of a single stiff layer debonding from the bottom of the multi-layer, with $E_1/E_2 = 1/3$ and $\nu_1 = \nu_2 = 0.33$.

Figure 6 provides a plot of normalized G vs a/h for a four-layer axisymmetric multi-layer with debonding at the mid-plane. The stiffness, $\bar{E}$, of the layers alternates with a ratio of 1 : 3. G for this axisymmetric problem exhibits behavior similar to that of G for the two-layer problems, increasing steadily with a/h and then reducing to zero as the crack tip approaches the center of the multi-layer. The difference in normalized G vs a/h behavior is evidenced in a local peak in G for short cracks for this four-layer axisymmetric problem. A similar peak is observed for the four-layer thin-wall (plane stress) planar problem, as can be seen in the data plotted in Fig. 6 denoted by planar delamination (plane stress). The reason for this behavior is the existence of low normalized energy release rates for long delamination cracks for this four-layer problem. For short cracks, the energy release rate behavior is the same for a given material combination and strain mismatch (regardless of the number and thickness of the layers). Thus, the short crack behavior of G vs a/h of this four-layer problem is the same as that for the two-layer case shown in Fig. 4. However, the

long crack energy release rate for this problem is low, causing the short crack behavior to overshoot the long crack portion of the energy release rate curve. The low energy release rates for long cracks exhibited in Fig. 6 are a consequence of the shape of the debonded halves of this four-layer part. The two debonded portions of this part remain curved (with a positive curvature) after delamination. The curvature of the debonded layers decreases the strain mismatch along the mid-plane interface, which decreases the energy released by debonding along the mid-plane. Because they are a consequence of curvature in debonded portions of a part, energy release rate peaks for short cracks are not observed in two-layer debonding configurations or in multi-layered configurations where one of the two debonded pieces is not curved. Figure 7 shows normalized G vs a/h for a single stiff layer debonding from the bottom of an axisymmetric four-layer part. Because the single stiff layer is not curved after debonding, the normalized G for long delamination cracks for this problem is relatively large and no peak in G is observed for short cracks.

The plot of Fig. 6 shows clear parallels between the planar and axisymmetric behavior of energy release rates in cases exhibiting energy release rate peaks for short cracks. Peaks in G for short cracks make it possible to get short crack initiation and arrest. However, because short crack energy release rate peaks are a consequence of small magnitudes of long crack energy release rates, they are a cause of concern only if they occur on comparatively brittle interfaces.

This study focuses on the behavior of G as a function of delamination crack length in multi-layers, but information about the mode mix of delamination cracks is also required because the critical energy release rate for interfacial debonding, G_c, is mode mix dependent. In interfacial fracture problems, mode mix may be defined in terms of the phase angle of the complex stress intensity factor, K (see Rice (1988) or Suo and Hutchinson (1990), for example). K is typically defined with respect to the stresses ahead of the crack tip, given by

$$\sigma_{yy}+i\sigma_{xy}=\frac{K}{\sqrt{2\pi x}}x^{i\varepsilon}, \tag{7}$$

where for materials 1 and 2

$$\varepsilon=\frac{1}{2\pi}\ln\left[\frac{\mu_1+\mu_2\kappa_1}{\mu_2+\mu_1\kappa_2}\right]. \tag{8}$$

The x and y coordinates used in eqn (7) are local crack tip coordinates, as shown in Fig. 1. In eqn (8), $\mu_j (j=1,2)$ is the material shear modulus, $\kappa_j=(3-\nu_j)/(1+\nu_j)$ $(j=1,2)$ for plane stress and $\kappa_j=(3-4\nu_j)$ $(j=1,2)$ for plane strain. K, the complex stress intensity factor, takes the dimensional form

$$K=K_1+iK_2=f\times(\text{stress})\times(\sqrt{h}h^{-i\varepsilon}), \tag{9}$$

where f is non-dimensional and, in general, a complex function of the material properties and the specimen geometry. The parameter h is the characteristic length of the problem. For a long delamination crack between layers of equal thickness, the characteristic length is the layer thickness, h. The mode mix of an interfacial crack can be specified by the angle ψ, defined as

$$\psi=\tan^{-1}\left[\frac{\mathrm{Im}(Kh^{i\varepsilon})}{\mathrm{Re}(Kh^{i\varepsilon})}\right]. \tag{10}$$

ψ is defined to be independent of h, the characteristic length, and can be considered as a consistent measure of the ratio of normal stress to shear stress ahead of the crack tip. Consideration of eqns (7) and (10) shows that ψ is the phase angle of the complex quantity $\sigma_{yy}+i\sigma_{xy}$ minus the phase angle of the quantity $(x/h)^{i\varepsilon}$.

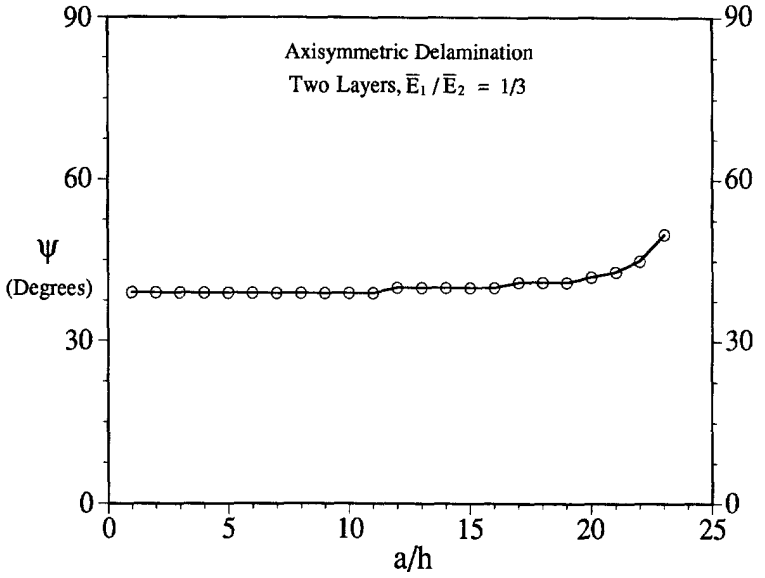

Fig. 8. Mode mix quantity, ψ vs normalized crack length for the two-layer axisymmetric delamination problem of Fig. 4 ($E_1/E_2 = 1/3$ and $\nu_1 = \nu_2 = 0.33$).

Figure 8 shows a plot of ψ vs a/h for a typical case of axisymmetric debonding of two layers with a stiffness ($\bar{E}$) ratio of 1 : 3 (energy release rates for this case are plotted in Fig. 4). The mode mix does not change significantly with crack length. As a result, for this problem energy release rates for all crack lengths can be compared to the same G_c value in designing delamination resistant multi-layers. This is in contrast to a more complicated problem in which both G and the mode mix (and thus G_c) change with crack length. In all of the cases presented in this study, modes of crack extension are essentially constant for crack lengths where G is steadily increasing.

In each of the axisymmetric delamination cases presented in this section, G increases steadily, reaching a value of G_{max} at a value of a/h that is problem dependent. This behavior is more complicated than the steady-state energy release rate behavior of planar problems. In the next section, a conservative upper bound for G_{max} for the axisymmetric problem is derived. The upper bound for G_{max} is given in terms of G_{ss} and G_{ss}^{plate} values for corresponding planar delamination problems and therefore can be calculated using only a residual stress model for the uncracked multi-layer.

5. ANALYSIS

In this section, a conservative upper bound for G_{max}, designated as G_{max}^{limit}, is determined for axisymmetric multi-layer delamination problems. A simple expression for G_{max}^{limit} is obtained by establishing links between axisymmetric and planar multi-layer delamination problems and using them within an approximation of energy release rate dependence on crack length. One link that can be made between axisymmetric and planar multi-layer delamination problems concerns the total potential energy released due to separation of a part into two pieces. Consider rectangular and circular multi-layers with the same layering geometry and the same differential thermal strains between layers, such as the problem illustrated in Figs 1b and 1c. In the rectangular plate problem of Fig. 1b, let $L = R$, where R is the radius of the circular multi-layer problem of Fig. 1c. Also, let the multi-layer width, B, equal πR, so that the planar area of the rectangular plate problem equals πR^2, the planar area of the circular multi-layer problem. Ignoring slight differences due to edge effects, for debonding along the same interface, the total potential energy released in separating this rectangular part (Fig. 1b) into two pieces must equal the total potential energy released in separating the circular-shaped part (Fig. 1c) into two pieces. The total potential energy released in separating the rectangular part can be expressed as

$$PE_{\text{total}} = B\int_0^L G\,\mathrm{d}a \approx \pi R^2 G_{ss}^{\text{plate}}, \tag{11}$$

where the approximate value of $\pi R^2 G_{ss}^{\text{plate}}$ is the debonded area multiplied by the steady-state energy release rate, which is accurate for parts having sufficiently large radii that regions close to the free edges are a small fraction of the part volume.

A second link that can be made between the planar and axisymmetric problems concerns the energy release rate behavior of relatively short axisymmetrically extending cracks. The crack lengths of concern are just outside the short crack regime, in the portion of the plot where energy release rates begin to increase steadily with crack length. If both radial and circumferential stresses were fully released, then the energy release rate just outside the short crack regime would equal G_{ss}^{plate}, the steady-state energy release rate of a rectangular plate (biaxial stress) planar delamination problem. As noted in the Numerical Results section, for short crack lengths an axisymmetrically extending crack will release radial stresses (σ_{rr}), but not circumferential stresses ($\sigma_{\theta\theta}$). This is due to circumferential constraint behind the crack front, in the debonded portions of the multi-layer. As a result, a uniaxial ($\sigma_{\theta\theta}$) state of stress is left behind the crack front as it advances. The steady-state energy release rate associated with the release of a uniaxial stress (such as $\sigma_{\theta\theta}$) is G_{ss}, the steady-state energy release rate for planar delamination of a thin-walled multi-layer (Fig. 1a). Thus the energy release rate accompanying the release of the stress σ_{rr} for short axisymmetrically extending cracks should be the difference in energy release rates of the biaxial and the uniaxial cases. This energy release rate, designated in this study as G_i, is thus equal to $G_{ss}^{\text{plate}} - G_{ss}$. In plots such as those of Figs 3–7, this should be the value the energy release rate approaches as the crack length is reduced, outside of the short crack regime. Values of G_i are provided in Figs 3–7, and the numerical results clearly approach G_i as the crack length is reduced (before falling to zero at $a/h = 0$).

The energy release rate behavior for axisymmetric problems is difficult to model for all crack lengths because of the complex manner in which the stresses σ_{rr} and $\sigma_{\theta\theta}$ are released. In order to determine a value for $G_{\max}^{\text{limit}}$, G is assumed to have a simple (yet representative) dependence on the normalized crack length a/h. Based on the plots of G/G_0 vs a/h of Figs 3–7, the energy release rate behavior for axisymmetric problems can be reasonably approximated as having a bilinear dependence on a/h. This bilinear approximation would consist of an initial value of G_i at $a/h = 0$, increasing linearly to $G_{\max}$ at a crack length of $a_{\max}$ and then falling to zero at $a = R$.

Use of a bilinear G vs a approximation would be reasonable, but would require specification of a problem-dependent value of $a_{\max}$. For a bilinear curve it can be shown, by varying the crack length ($a_{\max}$) at which G is maximum while keeping the total energy released due to debonding (related to the area under the G vs a curve) constant, that $G_{\max}$ is greatest for $a_{\max} = R$. Therefore, for the purpose of determining a conservative upper bound for $G_{\max}$, it is assumed that $a_{\max} = R$. This final assumption results in a linear approximation for energy release rate behavior, with values of G_i at $a = 0$ and $G_{\max}$ at $a = R$. The linear approximation for G vs a/h is thus given by the equation

$$G_{\text{linear}} = \frac{(G_{\max} - G_i)}{R/h}\,a/h + G_i, \tag{12}$$

where R is the multi-layer radius.

The total potential energy released for complete axisymmetric debonding of a circular multi-layer can be expressed as

$$PE_{\text{total}} = 2\pi h^2 \int_0^R \left(\frac{R-a}{h}\right) G\,\mathrm{d}(a/h). \tag{13}$$

Substituting G_{linear} for G in eqn (13) and equating with the approximate total energy released for planar debonding of the same multi-layer configuration (see eqn (11)) gives

Table 1. Normalized G_{max} and G_{max}^{limit} values for the axisymmetric cases in Figs 3–7

	Case	G_{max} (Actual)	a_{max}/h	G_{max}^{limit} (Predicted)
1.	Two Layers $\bar{E}_1/\bar{E}_2 = 1$, $R = 25h$	1.33	20	1.67
2.	Two Layers $\bar{E}_1/\bar{E}_2 = 1/3$			
	$R = 10h$	1.03	6	1.54
	$R = 25h$	1.18	19	1.54
	$R = 35h$	1.22	28	1.54
3.	Two Layers $\bar{E}_1/\bar{E}_2 = 1/40$, $R = 25h$	0.33	16	0.49
4.	Four Layers Mid-plane Debonding $\bar{E}_1/\bar{E}_2 = 1/3$, $R = 25h$	0.42	19	0.54
5.	Four Layers Stiff Layer Debonding from Bottom $\bar{E}_1/\bar{E}_2 = 1/3$, $R = 25h$	0.73	19	0.93

$$h^2\int_0^R 2\pi\left(\frac{R-a}{h}\right)\left[\frac{(G_{max}-G_i)}{R/h}a/h+G_i\right]\mathrm{d}(a/h) = \pi R^2 G_{ss}^{plate}. \tag{14}$$

Substituting for G_i, integrating and solving for G_{max} gives the following expression for G_{max}^{limit}:

$$G_{max}^{limit} = G_{ss}^{plate} + 2G_{ss} = 2G_{ss}\left(\frac{2-\nu}{1-\nu}\right), \tag{15}$$

an upper bound for G_{max} for the axisymmetric problem.

Comparison between values of G_{max}^{limit} and actual values of G_{max} from Figs 3–7 shows that the G_{max}^{limit} values are indeed conservative (see Table 1). For delamination problems with mild mismatches in elastic layer properties and for problems with large R, values for G_{max}^{limit} are close to the numerically determined G_{max} values. For problems with mild stiffness mismatches, this is due to values of a_{max} that are close to R. For problems with large R, values of G_{max} will approach G_{max}^{limit} as R is increased, because a larger portion of the G vs a curve is essentially linear, matching the G dependence on a that is assumed in deriving G_{max}^{limit}. For problems with extreme mismatches in elastic layer properties and for problems with small R, the predicted values are significantly higher than the actual G_{max} values. It should also be noted, however, that G values are quadratic in stress and if stress intensity factors are compared then the difference between actual and predicted values is less than that indicated in Table 1.

An upper bound for G has thus been determined for the axisymmetric multi-layer delamination problem based on known expressions for the steady-state energy release rates of corresponding planar problems. A fracture analysis of the axisymmetric problem is not required to determine this quantity. Calculated values for G_{max}^{limit} can be used to design delamination-resistant interfaces, where requiring that $G_{max}^{limit} < G_c$ will ensure that axisymmetric delamination does not occur on the interface under consideration.

6. CONCLUSIONS

The present work provides an in-depth study of residual stress-driven delamination in axisymmetric multi-layers, with specific attention given to the behavior of energy release rates. Principles developed can be used in a wide range of multi-layer debonding applications. In such problems, the non-uniform release of in-plane stresses causes the energy release rate to increase steadily, reaching a maximum value at a crack length that is problem

dependent. Numerical test cases presented in this study assume elastic behavior during residual stress build-up and uniform thermal contractions in each layer, but the methods outlined are applicable to any problem with residual stress distributions that are independent of r and θ coordinates. Based on simple potential energy arguments, a conservative upper bound has been determined for G_{max}, the maximum energy release rate for all delamination crack lengths. This upper bound, G_{max}^{limit}, is calculated in terms of steady-state energy release rates for corresponding planar configurations by relating axisymmetric and planar multi-layer debonding problems. Determination of G_{max}^{limit} does not require a fracture mechanics-based analysis, greatly simplifying the analysis and understanding of axisymmetric debonding problems. In combination with measured critical energy release rates, G_{max}^{limit} values can significantly aid the design of delamination-resistant multi-layer configurations.

Acknowledgements—The authors gratefully acknowledge the support of the National Science Foundation (grant no. CMS-9411005). The authors would like to thank John Hutchinson for his insightful comments about this problem. They would also like to thank Lee Weiss and Fritz Prinz for their input concerning applications of this work to layered manufacturing methods.

REFERENCES

Beuth, J. and Narayan, S. H. (1996) Residual stress-driven delamination in deposited multi-layers. *International Journal of Solids and Structures*, **33,** 65–78.

Chin, R. K., Beuth, J. L. and Amon, C. H. (1995) Control of residual thermal stresses in shape deposition manufacturing. In *Proceedings of the Solid Freeform Fabrication Symposium*. The University of Texas at Austin, August 1995, pp. 221–228.

Drory, M. D., Thouless, M. D. and Evans, A. G. (1988) On the decohesion of residually stressed thin films. *Acta Metallica*, **36,** 2019–2028.

Evans, A. G., Drory, M. D. and Hu, M. S. (1988) The cracking and decohesion of thin films. *Journal of Material Research*, **3,** 1043–1049.

Evans, A. G. and Hutchinson, J. W. (1984) On the mechanics of delamination and spalling in compressed films. *International Journal of Solids and Structures*, **20,** 455–466.

Hutchinson, J. W. and Suo, Z. (1991) Mixed mode cracking in layered materials. *Advances in Applied Mechanics*, Vol. 29, eds J. W. Hutchinson and T. Y. Wu. Academic Press, San Diego, pp. 63–191.

Hutchinson, J. W., Thouless, M. D. and Liniger, E. G. (1992) Growth and configurational stability of circular, buckle-driven film delaminations. *Acta Metallica*, **40,** 295–308.

Jensen, H. M. (1993) Energy release rates and stability of straight-sided, thin-film delaminations. *Acta Metallica*, **41,** 601–607.

Marcus, H. L. and Bourell, D. L. (1993) Solid freeform fabrication. *Advances in Material Processes*, **9,** 28–35.

Prinz, F. B., Weiss, L. E., Amon, C. H. and Beuth, J. L. (1995) Processing, thermal and mechanical issues in shape deposition manufacturing. In *Proceedings of the Solid Freeform Fabrication Symposium*, The University of Texas at Austin, August 1995, pp. 118–129.

Rice, J. R. (1988) Elastic fracture mechanics concepts for interfacial cracks. *Journal of Applied Mechanics*, **55,** 98–103.

Stringfellow, R. G. and Freund, L. B. (1993) The effect of interfacial friction on the buckle-driven spontaneous delamination of a compressed thin film. *International Journal of Solids and Structures*, **30,** 1379–1395.

Suo, Z. and Hutchinson, J. W. (1990) Interface crack between two elastic layers. *International Journal of Fracture*, **43,** 1–18.

Timoshenko, S. (1925) Bending and buckling of bimaterial strips. *Journal of the Optical Society of America*, **11,** 233–255.